ASME 2019 International Design Engineering Technical Conferences and Computers and Information in Engineering Conference
IDETC2019
August 18–21, 2019, Anaheim, California, USA

IDETC2019-97881

PSEUDO-RIGID BODY DYNAMIC MODELING OF COMPLIANT MEMBERS FOR DESIGN

Vedant
University of Illinois at Urbana-Champaign
Aerospace Engineering
Urbana, IL 61801
Email: vedant2@illinois.edu

James T. Allison
University of Illinois at Urbana-Champaign
Industrial & Enterprise Systems Engineering
Urbana, IL 61801
Email: jtalliso@illinois.edu

ABSTRACT

Movement in compliant mechanisms is achieved, at least in part, via deformable flexible members, rather than using articulating joints. These flexible members are traditionally modeled using Finite Element Models (FEMs). In this article, an alternative strategy for modeling compliant cantilever beams is developed with the objectives of reducing computational expense, and providing accuracy with respect to design optimization solutions. The method involves approximating the response of a flexible beam with an n-link/m-joint Pseudo-Rigid Body Dynamic Model (PRBDM). Traditionally, PRBDM models have shown an approximation of compliant elements using 2 or 3 revolute joints (2R/3R-PRBDM). In this study, a more general nR-PRBDM model is developed. The first n resonant frequencies of the PRBDM are matched to exact or FEM solutions to approximate the response of the compliant system. These models can be used for co-design studies of flexible structural members, and are capable of modeling higher deflection of compliant elements.

1 Introduction

Many complex engineering systems are comprised of multiple mechanical members to attain the desired functionality and performance. Recently, it has been shown that elastic compliance in individual members within a system can be exploited to reduce system complexity [1]. This can be achieved in part by utilizing compliance to create multifunctional components, which can help reduce the required number of discrete components. In addition, compliant mechanisms can help reduce overall volume, improve mechanical precision, and reduce wear.

Modeling such systems is a challenging task. There are several methods of varying fidelity to model the compliant members; some of the well-known methods include: Finite Element Analysis (FEA), lumped-parameter models, and Pseudo Rigid Body Models (PRBMs) [1]. Each of these methods has been shown to have individual strengths and weaknesses. Since many compliant structures undergo large deflection, techniques that approximate the performance of the compliant structure well for large deflection are desirable. PRBMs approximate the performance of a compliant member by modeling them as a series of rigid bodies linked to each other using torsional spring joints. PRBMs have been shown to model properties such as bistability/tristability [2, 3], dynamic behaviors [4, 5], and pose workspace [6].

Pseudo Rigid Body Dynamic Models (PRBDMs) are a variation of PRBMs, where the dynamic response of the model is matched to the expected response from the complaint system. The matching of system response can be performed using several metrics. Some of the existing approaches have utilized the deflection of a compliant member (e.g., a cantilever beam) under constant structural loads. Most initial studies explored the spring stiffness and the position of a single revolute joint (1R-PRBM) to approximate the dynamics [1]. The 1R-PRBM uses a characteristic pivot along the beam, used to approximate the response of any compliant member. Subsequent studies have explored more accurate approximation of the compliant members that undergo larger deflection levels using two revolute joint (2R) [7] and 3R PRBM models [8]. These models focused on mapping the deflection of a compliant member accurately. Most PRBMs are

load dependent, where the spring stiffness and joint position depend on the value and type of load applied. This is undesirable for a general model approximation. A survey of multiple PRBMs is provided in Ref. [9]

A comparison of the lumped parameter model against the FEA results for compliant members was performed previously, and it was discovered that the lumped model was more accurate in approximating deflection, whereas the FEA model was more effective at modeling resonant frequencies [10].

Co-design is a class of dynamic system design problems and methods of growing importance that aims to produce system-optimal designs by considering both physical and control system design decisions in an integrated manner [11–13]. Successful application of co-design methods requires the creation of low- to medium-fidelity models that predict the effect of changes both to physical and control system design decisions. Medium-fidelity models that do not depend on computationally expensive steps (e.g. re-meshing) are very desirable for co-design applications, such as compliant mechanisms and intelligent structures. In this study, a method of modeling a non-uniform cantilever beam using nR-link PRBDM models is introduced. The realized PRBDM models will have the same first 'n' resonant modes as the original beam. The natural frequency for this study is obtained using COMSOL[14] eigenvalue analysis, and the eigenvalue of the PRBDM equation is matched using an optimization scheme to find the system parameters that minimize the difference in the eigenvalues of the two systems. Alternate methods to obtain the resonant frequencies include use of analytical methods [15] and simple machine learning methods.

2 Problem Formulation

The PRBDM modeling method accuracy depends on obtaining appropriate values for spring stiffness, the number of joints, and the distance between joints. For design purposes, these model parameters must be estimated based on independent physical design variables, such as geometric parameters. This article investigates the utility of several strategies for mapping design variables to PRBDM parameters. Quantitative comparison of mapping strategies is based on candidate beams whose specifications are generated randomly, and where the first n eigenvalues are approximated using a variety of methods. These approximated eigenvalues are compared against "truth" values obtained for test beams using either analytical methods similar to those presented in Ref. [15], or an FEM eigenanalysis with a coarse mesh.

The dynamical equations for a nR-PRBDM is then formulated. Numerical optimization is used to match the eigenvalues for the PRBDM to the truth values. The cantilever beam, which is constrained to move in a 2D plane, can be approximated as an n-revolute joint rigid multi-body arm, as depicted in Fig 1. This study quantitatively compares several mapping strategies to determine the choice of spring stiffness and node distance to best match the eigenvalues. Here it is assumed that the panels have a maximum limit of 1 meter for length and width, while the thickness was limited to a minimum of 10 mm.

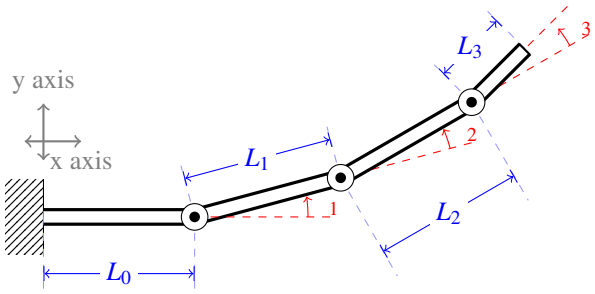

FIGURE 1: Illustration of 4-link/3R PRBDM

2.1 Generating random candidates

The mapping strategies are tested by applying them to randomly generated cantilever beams. The candidate beams are generated by first declaring the number of sections in the panel, denoted as an integer p. The generation steps include: choose p random numbers between 0 and 1, order these in ascending order, and append 0 and 1 to this list. These will serve as the X coordinates for the polygon representing distributed beam geometry (similar to the piecewise-linear design description used in Ref. [16]). The next step is to choose $p+2$ additional random real numbers between 0 and 1; these will serve as the Y coordinates for the polygon. Then, define a polygon where its starting point is the origin, its end point is point (0,1), and the start and end points are connected by a piecewise linear curve defined by vertices with positions specified by the ordered list of X and Y values. Reflecting the curve about the X-axis generates the closed polygon representing the planform geometry of

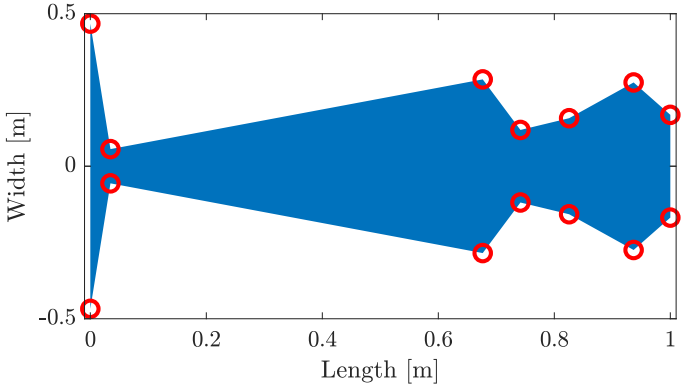

FIGURE 2: Visualization of a randomly generated beam, symmetric about X-axis (black line)

a candidate beam. Extruding this polygon to thickness t (in the Z-direction, out of the page) yields the complete description of a randomly generated test beam. All beams used in the tests here each have uniform thickness in the X-Y plane. One of the candidate panels is shown in Fig 2.

2.2 PRBDM Model

The dynamical model for an n-link arm in general can be represented by Eqn. (1). Assuming the beam is in a gravity-free environment, the contribution of $G(\ ;\ )$ is defined in Eqn. (2).

$$M(\ ;\ )\ddot{} + C(\ ;\dot{};\ )\dot{} + G(\ ;\ ) = \tag{1}$$

$$G(\ ;\ ) = K\ = \begin{bmatrix} K_{11} & \cdots & K_{1n} \\ \vdots & \ddots & \vdots \\ K_{n1} & \cdots & K_{nn} \end{bmatrix} \tag{2}$$

In the above equations, and $\dot{}$ are the local relative angular positions and velocities for each link. The quantities q and $\dot{q}$ correspond to the angular orientation and velocity of each link with respect to the global/world frame. The vector indicates the torque applied at each joint, and is the vector of design parameters for all links. Figure 1 shows an example of a 4 link/3R-PRBDM model. Here, $_n$ is the relative angle of the nth link with respect to the $(n-1)$th link. The relationship between and q is shown in Eqn. (3). The first link is always aligned to the world X axis, as quantified in Eqn. (4).

$$_j = q_j - q_{j-1};\ \forall\ j \in [1;2;\cdots;n] \tag{3}$$

$$q_0 = 0 \tag{4}$$

The matrix $C(\ ;\dot{};\ )$ in Eqn. (1) represents the Coriolis effect for the system, but an artificial damping term is added to the system to render the model more tractable for simulation. The modified $C_m(\ ;\dot{};\ )$ with damping is defined in Eqn. (5):

$$C_m(\ ;\dot{};\ ) = C(\ ;\dot{};\ ) + 0{:}1 \times \begin{bmatrix} 1 & 0 & 0 \\ 0 & 1 & 0 \\ 0 & 0 & 1 \end{bmatrix}: \tag{5}$$

The eigenvalues ( ) of the PRDBM model can calculated using Eqn. (6):

$$^2 = (M(\ ;\dot{};\ ))^{-1}K: \tag{6}$$

2.3 Mapping Strategy

The eigenfrequencies for the randomly-generated beams are obtained using `COMSOL` eigenvalue analysis. The eigenvalues and the mass participation factors are saved. The eigenvalues that have the highest mass participation in the Y direction are filtered and arranged in ascending order.

Numerical optimization is used to match the eigenvalues of an $(n+1)$-link/nR-PRBDM model to the truth values. The optimizer chooses the distance between the nodes L_j and each joint stiffness K_j, $j = 1;\cdots;n$, where n is the number of joints. A core

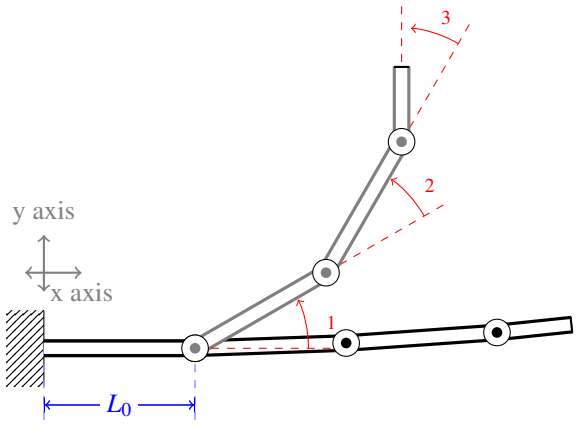

FIGURE 3: A 3R PRBDM at 2 different poses, the grey pose is the position when = + ×ones(1,3), and the black pose is for = ×ones(1,3)

challenge in this modeling problem is that the joint stiffnesses and eigenvalues depend on position via mass matrix dependence on pose. As a strategy to manage this variation in eigenvalues, we calculate for each design the eigenvalues across a range of poses. We generate this set of poses by sweeping across a range of joint position values $_i$ from small angles ( ) to =2, as depicted in Eqn. (7):

$$\hat{}_i = A_{i;<\cdot>} \tag{7}$$

where $\hat{}_i$ is the vector of all joint angles for pose i, and $A_{i;j}$ is an $m \times n$ matrix where the ith row corresponds to $\hat{}_i$. Specifically:

$$A_{i;<\cdot>} = [\ +i\ ;\cdots;\ +i\ ]; \tag{8}$$

where is small scalar offset value to prevent singular M (discussed below), and is small fixed angular value. Here is chosen such that at the mth pose, the end link world angle q_n is close to (but not exceeding) =2. Specifically, in the implementation here, = =2n. Other definitions of are possible.

The model given in Eqn. (1) was not tested for any cases where = 0, as this would result in a singular mass matrix (M). The pose for the PRBDM for the two boundary cases of $A_{0;<\cdot>}$ and $A_{m;<\cdot>}$ is shown in Fig. 3.

In the most general case, the stiffness of each joint is a continuous function of pose . To approximate this relationship in a discrete way, we define m different stiffness values for each joint. This results in $n \times m$ joint stiffness values required to specify a design.

In this study, a reduced-dimension stiffness representation is employed where a single stiffness correction parameter is found that allows us to define a single independent stiffness parameter for each joint, which then maps to m unique stiffness values for each joint for each pose. The rationale for this approach is that the stiffness variation on pose is modeled as a material property.

FIGURE 4: Plot of randomly generated beam, with physical properties for each section (link)

More specifically, the stiffness matrix in Eqn. (2) is assumed to be a diagonal matrix, as shown in Eqn. (9):

$$K = \begin{bmatrix} K_{11} & 0 & \cdots & 0 \\ 0 & K_{22} & \ddots & \vdots \\ \vdots & \ddots & \ddots & 0 \\ 0 & \cdots & 0 & K_{nn} \end{bmatrix} \tag{9}$$

To define an initial design for optimization, a unique K is assumed for each unique pose, of the same form as Eqn. (9). This yields m stiffness matrices; the elements of these matrices are defined according to Eqn. (10):

$$\hat{K}_i = \begin{bmatrix} K_{11}(i) & 0 & \cdots & 0 \\ 0 & K_{22}(i) & \ddots & \vdots \\ \vdots & \ddots & \ddots & 0 \\ 0 & \cdots & 0 & K_{nn}(i) \end{bmatrix} \tag{10}$$

$\hat{K}_i$ quantifies the stiffness for pose i, where the spring stiffness for each joint j and pose i, $K_{jj}(i)$, is approximated using a linear scaling to reduce the design representation dimension, according to Eqn. (11):

$$K_{jj}(i) = k_i \sqrt{\frac{EI_j}{\hat{m}_j}}; \tag{11}$$

where k_i is defined as a scaling parameter, also referred as stiffness correction factor, that is used as the independent stiffness design variable approximates how joint stiffness depends on pose. E is the material modulus of elasticity, I_j is the area moment of inertia for link j, and $\hat{m}_j$ is the mass of link j. This linear mapping strategy uses m independent design variable values for k_i, along with link mechanical properties, to generate m unique stiffness variables needed to define $\hat{K}_i$, $i = 1, \ldots, m$. Eqn. (9) is based on the assumption that the stiffness correction factor is a characteristic of the material and should not depend on the properties unique to each section.

The optimizer reduces the difference between the sorted eigenvalues from both systems (PRBDM and truth values, either FEM or exact) by minimizing the l_2 norm between the sorted eigenvalue vectors, as defined in Eqn. (12):

$$\| \lambda_{error}(k_i, \ldots, k_i) \|_2 = \| \lambda_{FEA} - \lambda_{PRBDM}(k_i, \ldots, k_i) \|_2 . \tag{12}$$

Here it is assumed that $\lambda_1 = 0$. The optimization problem formu-

lation for eigenvalue matching is defined in Eqn. (13):

$$\min_{L_j,k_i} \sum_{i=1}^{n} \| \text{error}(\lambda_i, 0, \lambda) \|_2 \quad (13a)$$

$$\text{subject to:} \quad \sum_{j=0} L_j = 1 \quad (13b)$$

$$L_j \geq 0.025, \quad (13c)$$

$$L_j \leq (1 - 0.025), \quad (13d)$$

where L_j is the length of the jth link (these values are independent of pose). This problem was solved using the Matlab[1] function fmincon with MultiStart to improve the probability of finding globally-optimal PRBDM parameter values.

The compliant beam model parameter vector α is a vector of length $(5+m)n$. Eqn. (14) details the components of α:

$$\alpha = [\theta, k, \hat{m}, J, X_{com}, Y_{com}]^T, \quad (14)$$

where θ is a vector (length m) of normalized link length values:

$$\theta_i = L_i / L_{total}, \quad L_{total} = \sum_i L_i = 1, \quad (15)$$

k is a vector (length m) of stiffness correction factors for each pose, $\hat{m}$ is a vector (length m) containing the mass of each link (assuming constant cross-section prismatic geometry), J is the vector of rotational mass moments of inertia for each link, and X_{com} and Y_{com} are the center-of-mass locations in the $i+1$th joint frame. Due to the symmetry assumption used here, all values for the vector Y_{com} are zero (at least with respect to numerical tolerances).

Once the number of joints has been chosen for the PRBDM to approximate the compliant member, independent components of α can be specified:

$$\alpha_{ind} = [\theta, k]^T. \quad (16)$$

These are then $n(1+m)$ independent beam design optimization variables based on the above PRBDM approximation and linear stiffness correction strategy. The next subsection describes how the remaining design parameters in α are calculated from α_{ind}.

2.4 Design Parameter Calculation

Once α_{ind} is specified, the optimization problem given in Eqn. (13) is solved using a multi-start approach with a gradient-based optimization algorithm. The set of start points are generated using a custom strategy, defined in Eqn. (17):

$$L = \text{random}(1, 100, n-1) \quad (17a)$$

$$\theta = \left[L, 1 - \sum L \right] / 100 \quad (17b)$$

$$k = \text{random}(m) \quad (17c)$$

where $L = [L_1, \ldots, L_{n-1}]$ is the vector of link lengths, random() is a uniform random number generator without replacement, θ is a normalized length vector based on the random length vector, and k is a randomly generated set of stiffness correction factors (length m). The numerical scaling defined in Eqn. (11) eases numerical solution difficulty due to differing orders of magnitude in the unscaled parameter space. In Eqn. (17a), the random function chooses $n-1$ unique random integers between 1 and 100. To sample a random uniform distribution under the simplex condition (Eqn. (13b)), the method described in Ref. [18] is used, as seen in Eqn. (17b).

Once the values of θ and k are known, the values of $\hat{m}$, J, X_{com}, and Y_{com} can be estimated using the first and second area moments of the sections of the polygons. During the optimization, for each new link length design, the physical properties for each link is calculated, and an updated α is obtained. The physical properties for each section is shown in Fig. 4 for a sample design.

Algorithm	fmincon , MultiStart [19–21]
Constraint Tolerance	1e-6
Step Tolerance	1e-6
Max Iterations	10000
Optimality Tolerance	1e-6
Max Function Evaluations	5000

TABLE 1 : Optimizer conditions

3 Test Problems

In this section, two cantilever beams are modeled using the PRBDM defined above. The first example models a uniform rectangular cantilever beam, while the second example corresponds to a randomly-generated beam. The material for the beam is Steel ANSI 4340, available in COMSOL [14].

The PRBDM model for 4-link and 5-link cases are used as candidate models to match the first 4 (and 5) modes, respectively. The optimal stiffness correction factor k_i and joint separation L_j is obtained by solving the optimization problem in Eqn. 13 using the algorithm settings shown in Table 1.

3.1 Test Problem 1: Uniform Rectangular Beam

A uniform rectangular beam is considered for validation of the methods. The test beam used the parameters listed in Table 2.

The PRBDM method is used to find the response of the model and compare the result against the analytical solutions for a uniform beam. The analytical solutions are obtained us-

[1] The Matlab code for these test problems is available in Ref. [17].

Length[m]	Width[m]	Thickness[m]
1	0.3624	0.040532

TABLE 2: Uniform beam parameters

ing the Euler Bernoulli beam theory for cantilever plates, based on Eqn. (18), from Ref. [22]. An illustration of a simple beam is shown in Fig 5, and the natural frequency for the bending mode is de ned as:

$$\omega_n = \beta_n^2 \sqrt{\frac{EI}{AL^4}} = \beta_n^2 \sqrt{\frac{E\frac{bh^3}{12}}{(bh)L^4}} \qquad (18)$$

where E is the material modulus of elasticity, I is the beam area moment of inertia about the root, ρ is the beam material density, A is the uniform beam cross-sectional area, L is the beam length, and β_n is the coe cient for the nth resonance mode. The value of β_n is obtained by solving Eqn. (19). The rst three solutions to this equation are listed in Eqn. (20), where the rst value corresponds to the rst bending mode, the second value to the second mode, and so on. The rst two mode shapes are illustrated in Fig 5, labeled as ϕ_1 and ϕ_2.

$$1 = \cos(\beta_n)\cosh(\beta_n) \qquad (19)$$

$$\beta_n = [1.875; 4.694; 7.855; \ldots] \qquad (20)$$

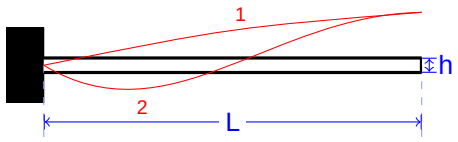

FIGURE 5: Side-view of a uniform beam of length L, thickness h, and width b. The red curves show the rst 2 bending modes of the cantilever beam

Maximum element size	0.03 m
Minimum element size	0.001 m
Maximum element growth rate	1.5
Curvature factor	0.3
Resolutions of narrow regions	0.9

TABLE 3: Mesh generation parameters [14].

FIGURE 6: Mesh for random panel used for FEM analysis

3.2 Test Problem 2: Random Beam

A random beam is generated using the procedure stated in Sec. 2, for $p = 10$. The randomly generated beam used for the studies presented here is shown in Fig. 2. COMSOL was used to estimate the rst 40 natural frequencies for the beam along with the mass participation factors (MPF) for each mode. A 'ne' mesh is used to estimate the resonant frequencies, as shown in Fig. 6, according to the parameters mentioned in Table 3 . The coarse mesh supports computationally e cient estimation of the resonant frequencies. The resonant frequencies are then ltered according to the MPF to obtain the modes that exhibit bending along the desired axis; Fig. 13 shows the top 12 ltered modes. The vector of 5 eigenvalues obtained for the panel from Fig. 2, using the mesh shown in Fig. 6, is presented in Eqn. (21).

$$\omega_{panel} = \begin{bmatrix} 55.037; & 414.59; & 1122; & 2189; & 3641.5 \end{bmatrix}^T \qquad (21)$$

4 Results and Discussions

In this section, the results for the two test cases are discussed. The rst case maps the resonant values for a uniform cantilever beam to a 3R-PRBDM and 4R-PRBDM, while mapping the rst three eigenvalues. The second case discusses one of the randomly generated random beams. The PRBDM matching code, which is available at Ref. [17], was solved for 50,000 di erent model beams; the beam discussed here is beam number 17,572[2]. The beam was modeled using a 4R-PRBDM and a 5R-PRBDM for di erent number of eigenvalues.

4.1 Uniform beam

This case uses the Matlab fmincon function with MultiStart . The problem was solved based on the dimension-reduction strategy discussed above. One of the initial points used for the optimizer was based on uniform space, as

[2]The remaining data will be available upon nal publication via an archival data repository.

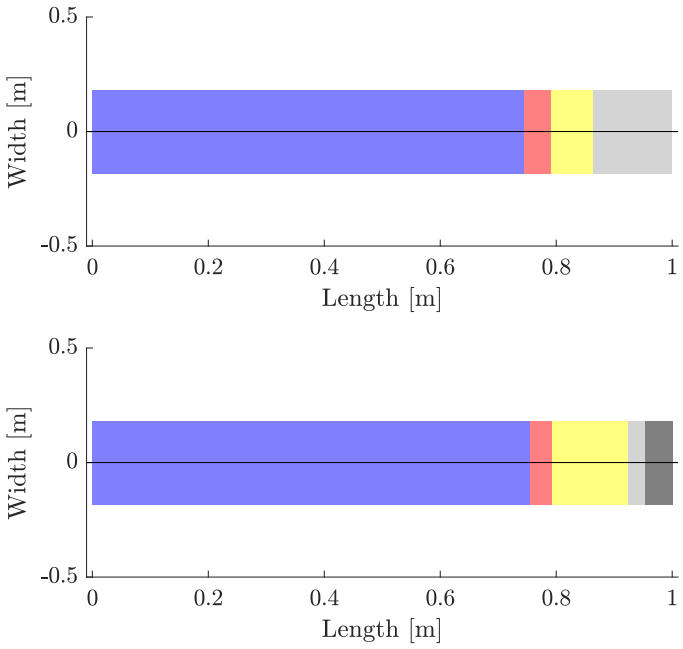

FIGURE 7: Plot of uniform beam, with optimal joint separation. Shaded regions indicate distinct rigid links.

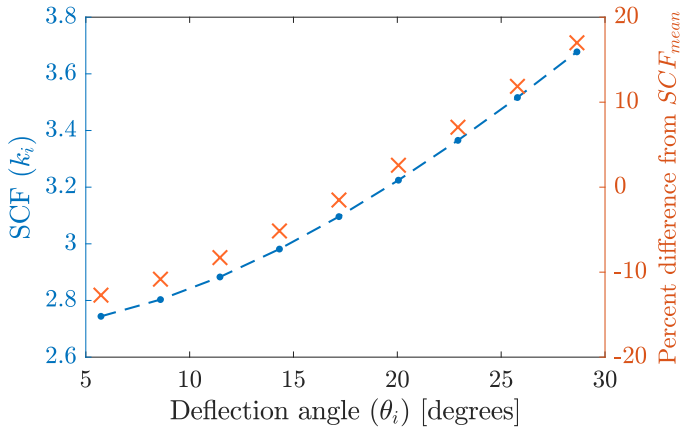

FIGURE 8: Plot of the spring Stiffness Correction Factor (SCF) vs. deflection angle (in degrees), for the 4R-PRBDM uniform beam. The right-hand axis corresponds to the relative change from mean values (Eqn. 24).

defined in Eqn. (22):

$$_i = \frac{L}{n}; \tag{22a}$$

$$k_i = 1: \tag{22b}$$

The results for the 3R-PRBDM and 4R-PRBDM can be seen in Fig. 7. An interesting observation here is that the length fraction

Joints	Frequencies mapped	Stiffness correction factor	Joint distance[m]	Loss [%]
3	3	2:7441 2:8032 2:8830 2:9815 3:0960 3:2246 3:3652 3:5164 3:6776	0:7447 0:0466 0:0725 0:1362	0.0168
4	3	3:2301 3:2812 3:3504 3:4356 3:5349 3:6462	0:7555 0:0369 0:1323 0:0281 0:0472	0.0168

TABLE 4: Results for uniform beam

for the first joint $_1$ is relatively similar for both cases. This is similar to the “characteristic length" for a 1R-PRDBM described in [9].

The variation of the spring Stiffness Correction Factor (SCF) with respect to different poses for the 3R-PRBDM case can be seen in Fig. 8. The right-hand side y-axis shows the percent difference between the SCF for the given joint angles to the mean SCF. The mean SCF is defined by Eqn. 23. The variation of the spring stiffness is small, but shows a close to linear trend.

$$\text{SCF}_{\text{mean}} = \frac{1}{m} \sum_{i=0}^{m} k_i \tag{23}$$

$$P_i = \frac{k_i - \text{SCF}_{\text{mean}}}{\text{SCF}_{\text{mean}}} 100 \tag{24}$$

Both the 3R-PRDBM and 4R-PRBDM models were used to map the first three resonant modes of the beam to the PRBDM. The details of the solution obtained for both cases can be seen in Table. 4. The “Loss" column shoes the value of the objective function Eqn. 12.

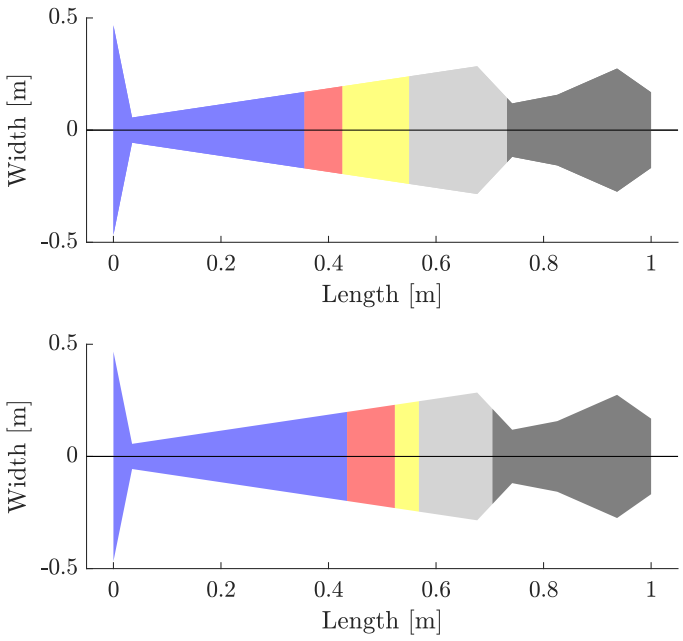

FIGURE 9: Plot of randomly general beam, with physical properties for each section optimized for eigenvalue matching (4R-PRBDM)

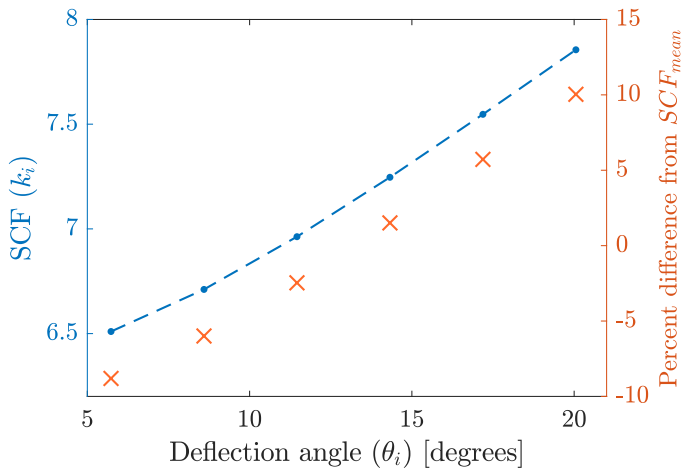

FIGURE 10: Plot of the spring Stiffness Correction Factor (SCF) vs. deflection angle (in degrees), for the 4R-PRBDM random beam case. The right-hand axis corresponds to the relative change from mean values (Eqn. 24).

4.2 Random Beam

The random beam was solved for both the 4R-PRBDM and the 5R-PRBDM cases. Both cases were solved to map the first three eigenfrequencies as well as the maximum number of eigenfrequencies that the models allow. The results for the random beam are thus divided into two sections, one for the 4R-PRBDM, and the latter for the 5R-PRBDM.

4.2.1 4R-PRBDM Approximation The optimization problem to solve for the joint distribution and spring stiffness was initialized using 1,024 unique initial points, and solved using the `MultiStart` algorithm in `Matlab`. One of the initial beam designs is illustrated in Fig 4. The value chosen for this study was 0.1, and is 0.05, for Eqn. (7).

The optimizer solves for both the link lengths and SCFs simultaneously to best match the eigenvalues. For the 4R-PRBDM model, the optimizer converged to the solution shown in Fig 9. The obtained PRBDM model has eigenvalues which differ by 0.12% of the eigenfrequencies obtained using `COMSOL`. Similar to the uniform beam case, the length fraction for both cases of the 4R-PRBDM ($_1$) are indicative of a "characteristic pivot" for this non-uniform and higher-dimensional (4R-PRBDM) case.

The SCF for each deflection case is shown in Fig 10. A linear trend is observed for the correction factor with respect to the angle of deflection between each link. A summary of solution parameters can is provided in Table 5.

When the SCF is applied according to Eqn. (11), the spring stiffness is obtained for different deflection angles. The spring stiffness values for each deflection case can be seen in Eqn. (25).

$$K_{4R}^{q1} = 10^5 \times \begin{bmatrix} 1{:}2089 & 2{:}1401 & 2{:}9362 & 4{:}8353 \end{bmatrix} \quad (25a)$$

$$K_{4R}^{q2} = 10^5 \times \begin{bmatrix} 1{:}2462 & 2{:}2062 & 3{:}0269 & 4{:}9846 \end{bmatrix} \quad (25b)$$

$$K_{4R}^{q3} = 10^5 \times \begin{bmatrix} 1{:}2930 & 2{:}2890 & 3{:}1405 & 5{:}1717 \end{bmatrix} \quad (25c)$$

$$K_{4R}^{q4} = 10^5 \times \begin{bmatrix} 1{:}3456 & 2{:}3822 & 3{:}2684 & 5{:}3823 \end{bmatrix} \quad (25d)$$

$$K_{4R}^{q5} = 10^5 \times \begin{bmatrix} 1{:}4015 & 2{:}4810 & 3{:}4040 & 5{:}6057 \end{bmatrix} \quad (25e)$$

$$K_{4R}^{q6} = 10^5 \times \begin{bmatrix} 1{:}4587 & 2{:}5824 & 3{:}5431 & 5{:}8346 \end{bmatrix} \quad (25f)$$

4.2.2 5R-PRBDM Approximation For the 5R-PRBDM model, the optimizer converged to the solution shown in Fig. 11. The obtained PRBDM model has eigenvalues which differ by 0.2277% of the eigenfrequencies obtained using `COMSOL`. This is higher than the value for a 4R-PRBDM model, but it must be noted that the 5R-PRBDM model maps 5 eigenfrequencies instead of 4. When 4 eigenfrequencies are mapped using a 5R-PRBDM the accuracy of the model is within 0.012%. The SCF for each deflection case is shown in Fig 12. Although a similar linear trend is observed for the correction factor with respect to the angle of deflection between each link, as with the 4R case, the variation is significantly smaller. A summary of solution parameters can be seen in Table 6. The unscaled spring stiffness for mapping the first 5 eigenfrequencies

can be seen in Eqn. (26).

$$K_{5R}^{q1} = 10^4 \times \begin{bmatrix} 9{:}3878 & 3{:}8301 & 2{:}4465 & 2{:}2160 & 1{:}2217 \end{bmatrix} \quad (26a)$$

$$K_{5R}^{q2} = 10^4 \times \begin{bmatrix} 9{:}4145 & 3{:}8410 & 2{:}4535 & 2{:}2223 & 1{:}2252 \end{bmatrix} \quad (26b)$$

$$K_{5R}^{q3} = 10^4 \times \begin{bmatrix} 9{:}4515 & 3{:}8561 & 2{:}4631 & 2{:}2310 & 1{:}2300 \end{bmatrix} \quad (26c)$$

$$K_{5R}^{q4} = 10^4 \times \begin{bmatrix} 9{:}4988 & 3{:}8754 & 2{:}4754 & 2{:}2422 & 1{:}2361 \end{bmatrix} \quad (26d)$$

$$K_{5R}^{q5} = 10^4 \times \begin{bmatrix} 9{:}5560 & 3{:}8988 & 2{:}4904 & 2{:}2557 & 1{:}2436 \end{bmatrix} \quad (26e)$$

5 Conclusion and Future Work

In this article, a strategy to approximate the dynamic behavior of compliant members using a reduced-order model. These models are particularly useful for design optimization, as computational expense can be reduced significantly while maintaining reasonable accuracy. Quantification of this tradeoff with respect to design solution accuracy is a topic for future work. Two test cases are presented, but the method has been validated for a large variety of beams. These results and the associated code are available at Ref. [17]. Some preliminary correlation of the spring stiffness is seen with the deflection angles, and the stiffness scaling was sufficient for a linear correlation between the stiffness correction factor and deflection angles. Some evidence of characteristic pivot distances has also been observed for both the uniform beam and the random beam cases. The correlation of the joint distances with the beam shape needs further investigation to show dependence.

More extensive studies that optimize the reduced-order PRBDM models for an enumerated distribution of joint separation could help generate empirically-driven analytic rules to de-

Frequencies mapped	Stiffness correction factor	Join distance[m]	Loss [%]
4	$\begin{bmatrix} 6{:}5099 \\ 6{:}7109 \\ 6{:}9627 \\ 7{:}2464 \\ 7{:}5471 \\ 7{:}8553 \end{bmatrix}$	$\begin{bmatrix} 0{:}3553 \\ 0{:}0707 \\ 0{:}1242 \\ 0{:}1819 \\ 0{:}2678 \end{bmatrix}$	0.1001
3	$\begin{bmatrix} 5{:}0093 \\ 5{:}2555 \\ 5{:}5703 \\ 5{:}9349 \\ 6{:}3344 \\ 6{:}7601 \end{bmatrix}$	$\begin{bmatrix} 0{:}4345 \\ 0{:}0890 \\ 0{:}0447 \\ 0{:}1366 \\ 0{:}2952 \end{bmatrix}$	0.0536

TABLE 5: Results for 4R-PRBDM, random beam

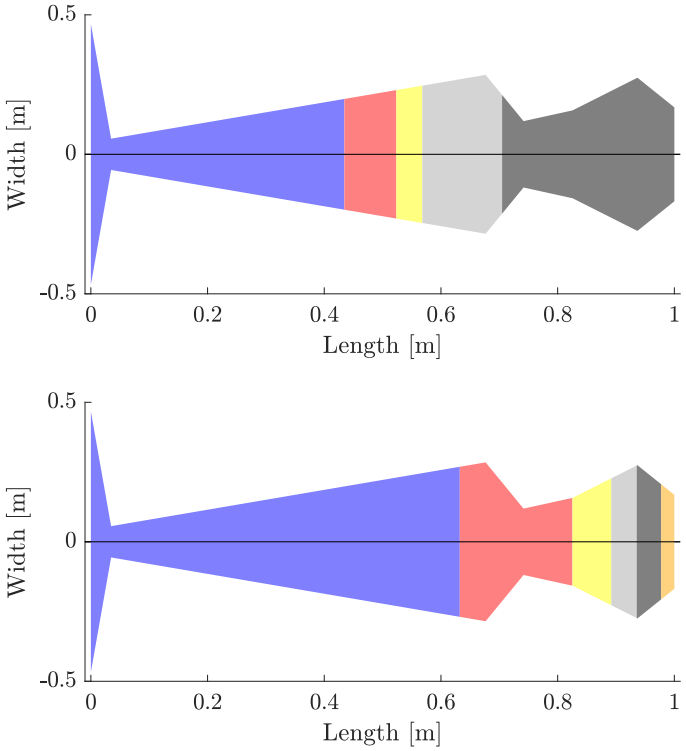

FIGURE 11: Plot of randomly general beam, with physical properties for each optimal section (5R-PRBDM)

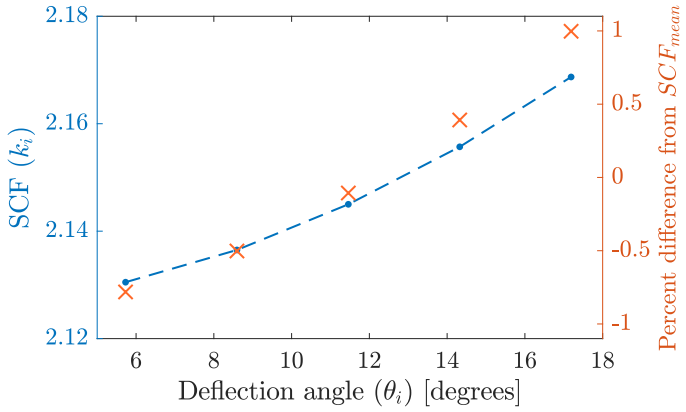

FIGURE 12: Plot of Spring Stiffness Correction Factor (SCF) vs. deflection angle (in degrees), for the 5R-PRBDM random beam case

Frequencies mapped	Stiffness correction factor	Join distance[m]	Loss [%]
5	2:1305 2:1365 2:1450 2:1557 2:1687	0:6323 0:1930 0:0667 0:0435 0:0418 0:0228	0.2277
3	3:3366 3:4041 3:4950 3:6062 3:7352	0:6632 0:0165 0:0844 0:1595 0:0093 0:0671	0.0119

TABLE 6: Results for 5R-PRBDM for random beam

termine link lengths and spring stiffness factors. If validated, this would eliminate the need to solve an optimization problem based on truth data, speeding up the implementation of effective PRBDMs for design studies. An efficient method for estimating the resonant frequencies could be obtained using a machine learning framework. Additionally, a reinforcement learning method could be used to train a neural network to provide the joint separation and spring stiffness for PRBDMs across a range of designs.

6 Acknowledgements

This material is based upon work partially supported by the National Science Foundation under Grant No. CMMI-1653118 and partially through the NASA SBIR in collaboration with CU aerospace Contract No. NNX17CA25P.

The authors would like to thank Daniel R. Herber for his guidance with this study.

References

[1] Howell, L. L., 2001. *Compliant mechanisms*. John Wiley & Sons.

[2] Jensen, B. D., and Howell, L. L., 2003. "Identification of compliant pseudo-rigid-body four-link mechanism configurations resulting in bistable behavior". *Journal of Mechanical Design,* ***125***(4), pp. 701–708.

[3] Chen, G., Wilcox, D. L., and Howell, L. L., 2009. "Fully compliant double tensural tristable micromechanisms (dttm)". *Journal of Micromechanics and Microengineering,* ***19***(2), p. 025011.

[4] Lyon, S., Erickson, P., Evans, M., and Howell, L., 1999. "Prediction of the first modal frequency of compliant mechanisms using the pseudo-rigid-body model". *Journal of Mechanical Design,* ***121***(2), pp. 309–313.

[5] Yu, Y.-Q., Howell, L. L., Lusk, C., Yue, Y., and He, M.-G., 2005. "Dynamic modeling of compliant mechanisms based on the pseudo-rigid-body model". *Journal of Mechanical Design,* ***127***(4), pp. 760–765.

[6] Midha, A., Howell, L. L., and Norton, T. W., 2000. "Limit positions of compliant mechanisms using the pseudo-rigid-body model concept". *Mechanism and Machine Theory,* ***35***(1), pp. 99–115.

[7] Kimball, C., and Tsai, L.-W., 2002. "Modeling of flexural beams subjected to arbitrary end loads". *Transactions-american Society of Mechanical Engineers Journal of Mechanical Design,* ***124***(2), pp. 223–235.

[8] Su, H.-J., 2009. "A pseudorigid-body 3R model for determining large deflection of cantilever beams subject to tip loads". *Journal of Mechanisms and Robotics,* ***1***(2), p. 021008.

[9] Chen, G., Xiong, B., and Huang, X., 2011. "Finding the optimal characteristic parameters for 3r pseudo-rigid-body model using an improved particle swarm optimizer". *Precision Engineering,* ***35***(3), pp. 505–511.

[10] Chudnovsky, V., Mukherjee, A., Wendlandt, J., and Kennedy, D., 2006. "Modeling flexible bodies in simmechanics". *MatLab Digest,* ***14***(3).

[11] Fathy, H. K., Reyer, J. A., Papalambros, P. Y., and Ulsov, A., 2001. "On the coupling between the plant and controller optimization problems". In Proceedings of the 2001 American Control Conference.(Cat. No. 01CH37148), Vol. 3, IEEE, pp. 1864–1869.

[12] Allison, J. T., and Herber, D. R., 2014. "Multidisciplinary design optimization of dynamic engineering systems". *AIAA Journal,* ***52***(4), Apr., pp. 691–710.

[13] Herber, D. R., and Allison, J. T., 2019. "Nested and simultaneous solution strategies for general combined plant and control design problems". *ASME Journal of Mechanical Design,* ***141***(1), Jan., p. 011402.

[14] AB, C., 1998. Comsol multiphysics v. 5.3. [Online]. Available: www.comsol.com.

[15] Herrera-May, A. L., Aguilera-Cortés, L. A., Plascencia-Mora, H., Rodríguez-Morales, Á. L., and Lu, J., 2011. "Analytical modeling for the bending resonant frequency of multilayered microresonators with variable cross-section". *Sensors,* ***11***(9), pp. 8203–8226.

[16] Chilan, C. M., Herber, D. R., Nakka, Y. K., Chung, S.-J., Allison, J. T., Aldrich, J. B., and Alvarez-Salazar, O. S., 2017. "Co-design of strain-actuated solar arrays for spacecraft precision pointing and jitter reduction". *AIAA Journal,* ***55***(9), Sept., pp. 3180–3195.

[17] Vedant. PRBDM code repository. [Online]. Available: https://github.com/VedantFNO/PRDBM_IDETC2019_97881.

[18] Smith, N. A., and Tromble, R. W., 2004. "Sampling uniformly from the unit simplex". *Johns Hopkins University, Tech. Rep,* ***29***.

[19] MultiStart. [Online]. Available: https://www.mathworks.com/help/gads/multistart.html.

[20] Ugray, Z., Lasdon, L., Plummer, J., Glover, F., Kelly, J., and Martí, R., 2007. "Scatter search and local nlp solvers: A multistart framework for global optimization". *INFORMS Journal on Computing,* ***19***(3), pp. 328–340.

[21] Glover, F., 1998. "A template for scatter search and path relinking". *Lecture notes in computer science,* ***1363***, pp. 13–54.

[22] Plunkett, R., 1963. "Natural frequencies of uniform and non-uniform rectangular cantilever plates". *Journal of Mechanical Engineering Science,* ***5***(2), pp. 146–156.

7 Appendix

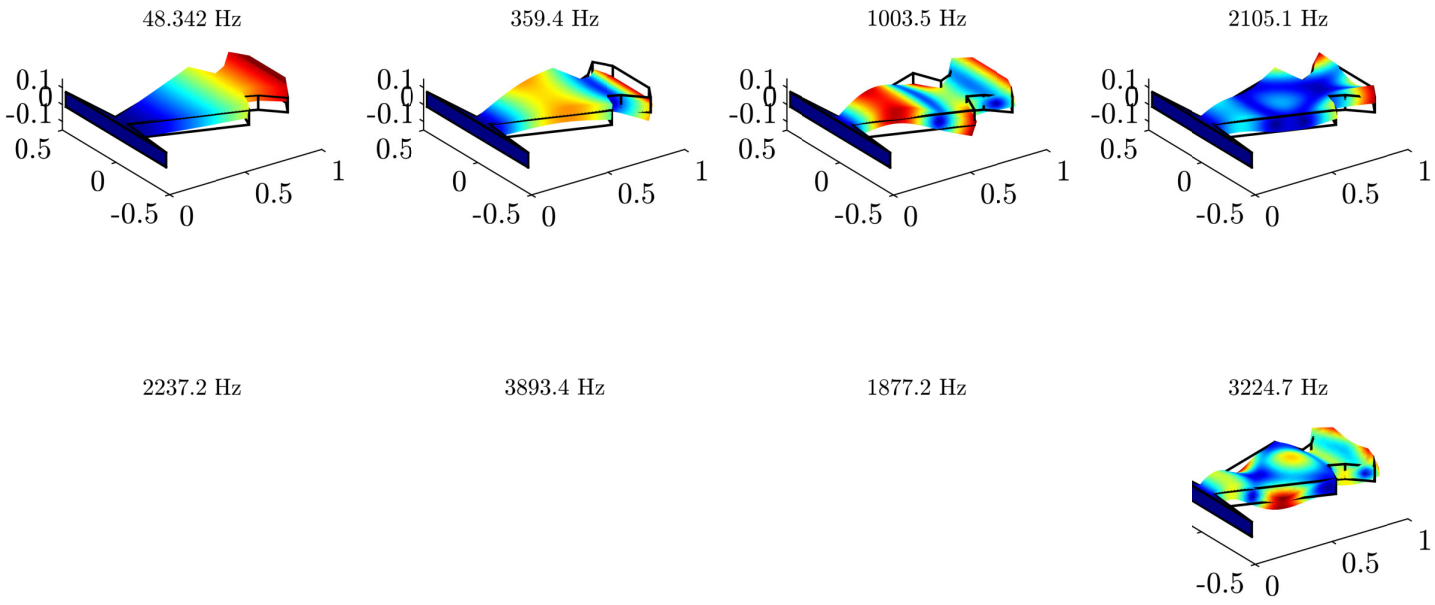

FIGURE 13: Plot of bending modes for 16 filtered eigenvalues, the title for each plot shows the resonant frequency, all axis lengths are in meters